Porous Nitride Light-Emitting Diodes

Nuño Amador-Mendez, Tiphaine Mathieu-Pennober, Stéphane Vézian, Marie-Pierre Chauvat, Magali Morales, Pierre Ruterana, Andrey Babichev, Fabien Bayle, François Julien, Sophie Bouchoule, et al.

Porous nitride light emitting diodes

Journal:	*ACS Photonics*
Manuscript ID	ph-2021-01729c
Manuscript Type:	Article
Date Submitted by the Author:	10-Nov-2021

Complete List of Authors:	Amador, Nuño; Centre de Nanosciences et de Nanotechnologies (C2N), Univ. Paris-Saclay Mathieu , Tiphaine ; Centre de Nanosciences et de Nanotechnologies (C2N), Univ. Paris-Saclay Vézian, Stéphane; Université Côte d'Azur Chauvat , Marie-Pierre ; Centre de Recherche sur les Ions les Matériaux et la Photonique Morales, Magali; Centre de Recherche sur les Ions les Matériaux et la Photonique Ruterana, Pierre; Centre de Recherche sur les Ions les Matériaux et la Photonique, SIFCOM, UMR6176 Babichev, Andrey; Saint Petersburg Electrotechnical University "LETI"; ITMO University Bayle, Fabien; Centre de Nanosciences et de Nanotechnologies (C2N), Univ. Paris-Saclay Julien, François H.; Centre de Nanosciences et de Nanotechnologies (C2N), Univ. Paris-Saclay Bouchoule, Sophie ; Centre de Nanosciences et de Nanotechnologies (C2N), Univ. Paris-Saclay Collin, Stéphane; Centre de Nanosciences et de Nanotechnologies (C2N), Univ. Paris-Saclay Gil, Bernard; Universite de Montpellier, Laboratoire Charles Coulomb Tappy, Nicolas ; Ecole Polytechnique Federale de Lausanne, Laboratory of Semiconductor Materials, Institute of Materials, Faculty of Engineering Fontcuberta i Morral, Anna; Ecole Polytechnique Federale de Lausanne Institut des neurosciences, Laboratoire des Matériaux Semiconducteurs Damilano, Benjamin; Université Côte d'Azur Tchernycheva, Maria; Centre de Nanosciences et de Nanotechnologies (C2N), Univ. Paris-Saclay

Porous nitride light emitting diodes

Nuño Amador-Mendez[1], Tiphaine Mathieu-Pennober[1], Stéphane Vézian[2], Marie-Pierre Chauvat[3], Magali Morales[3], Pierre Ruterana[3], Andrey V. Babichev[4,5], Fabien Bayle[1], François H. Julien[1], Sophie Bouchoule[1], Stéphane Collin[1], Bernard Gil[6], Nicolas Tappy[7], Anna Fontcuberta i Morral[7,8], Benjamin Damilano[2], and Maria Tchernycheva[1]

[1] Centre de Nanosciences et de Nanotechnologies (C2N), Univ. Paris-Saclay, UMR 9001 CNRS, Palaiseau 91120, France

[2] Université Côte d'Azur, CNRS, CRHEA, Valbonne 06560, France

[3] Centre de Recherche sur les Ions, les Matériaux et la Photonique, CIMAP-ENSICAEN, UMR 6252, Caen 14050, France

[4] Saint Petersburg Electrotechnical University "LETI", St. Petersburg 197022, Russia

[5] ITMO University, St. Petersburg 197101, Russia

[6] Laboratoire Charles Coulomb, UMR 5221 CNRS, Univ. Montpellier, Montpellier 34095, France

[7] Laboratory of Semiconductor Materials, Institute of Materials, Faculty of Engineering, Ecole Polytechnique Fédérale de Lausanne, Lausanne 1015, Switzerland

[8] Institute of Physics, Faculty of Basic Sciences, Ecole Polytechnique Fédérale de Lausanne, Lausanne 1015, Switzerland

KEYWORDS: *light emitting diode, porous material, InGaN, cathodoluminescence, electron beam microscopy, metal organic chemical vapor deposition, nanoscale analyses*

ABSTRACT: A porous InGaN/GaN blue light emitting diode is demonstrated using selective area sublimation. Transmission electron microscopy reveals that the structure is porous down to the Si substrate, however the porosity is higher in the GaN buffer, while smaller pores are observed in the active region. This change of porosity between the active region and the buffer is explained by the modification of the dislocation pattern in the heterostructure, which is evidenced by weak beam transmission electron microscopy on a non-porosified reference sample. Cathodoluminescence mapping and electron beam induced current microscopy (EBIC) analyses are used to probe the impact of porosification on the optical and electrical properties of the structure at nanoscale dimensions. It is observed that neither the quantum well emission nor the p-n junction EBIC spatial profile were degraded after porosification with respect to the non-annealed reference sample. A light emitting diode with a fully porous active region is fabricated using parylene pore filling for electrical insulation and its electroluminescence is analyzed.

Porosification of semiconductors as a way to control their optical and electrical properties have been studied in different materials since many years.[1,2] In nitrides, additional interest of porosification stems from the strain and dislocation density reduction when using porosified buffer layers.[3–6] This property is particularly important for nitride growth on Si substrates, for which the mismatch of thermal expansion coefficients and the dislocation issues are severe.

Due to the low cost and large size of Si substrates, growing nitride light emitting diodes (LEDs) on Si can significantly reduce the fabrication cost and thus boost the solid-state lighting. However, strain management to achieve high quality GaN layers on Si requires the growth of very complex structures, which increases the fabrication cost and lessens the interest of using Si. To solve this issue, porosification was proposed as an attractive alternative to accommodate the strain. Nitride layers can be porosified by using wet etching by HF or KOH,[4] reactive ion etching[7] or electrochemical etching (ECE) and photoelectrochemical etching (PECE).[6] LEDs grown on porous nitride buffer layers were reported showing improvement of their performance.[5,6,8]

Recently we have demonstrated that porous GaN can also be obtained by selective area sublimation.[9,10] This method is based on the strong difference of stability between the (0001) polar plane and the perpendicular non-polar ones such as {1-100} (m-planes) and {11-20} (a-planes). We have demonstrated that the porosification increases the luminescence efficiency in GaN bulk layers and in InGaN/GaN quantum wells grown on Si.[9] Part of this enhancement can be explained by a better light extraction (estimated to yield a signal increase by a factor of 3), however the observed luminescence improvement was much stronger (two-to-three orders of magnitude), attributed to the sublimation of defective regions with a strong non-radiative recombination.[9] Until now, all the reported LEDs exploiting the porosification use a porous buffer, while the active region itself remains non-porous. The use of porous layers in the device active region was only reported once with a demonstration of a fully porous p-n diode.[11] No InGaN-based devices exploring the effect of porosification through the active region has been investigated.

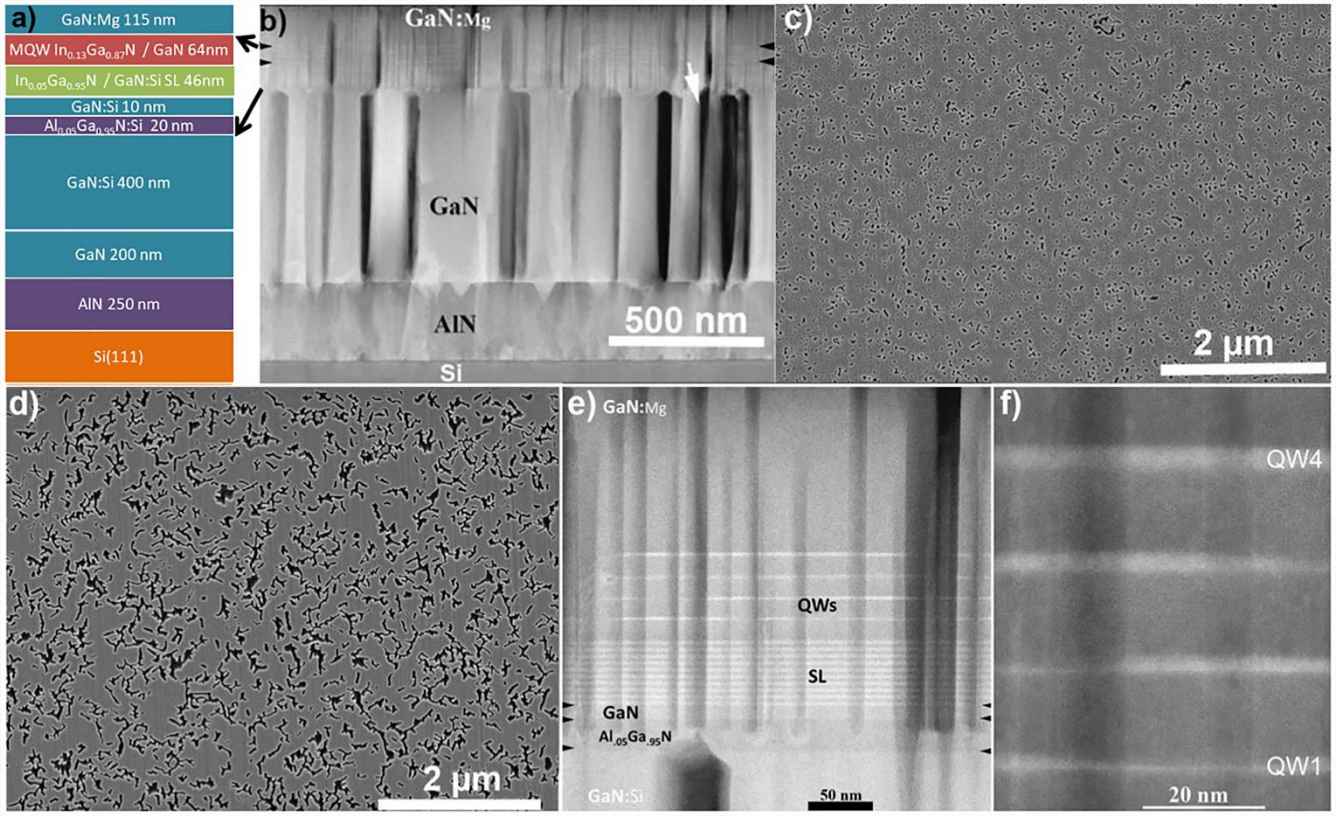

Figure 1. (a) Schematics of the LED structure, thicknesses of the various layers are displayed. (b) Low magnification STEM image of the whole heterostructure from the Si substrate to GaN:Mg surface layer after sublimation. (c) Plane-view SEM close to the surface region (d) SEM plane-view in the GaN buffer. (e) Cross-sectional view of the active QWs and the superlattice. (f) High magnification STEM image of the active InGaN/GaN QWs.

The purpose of the present study is to analyse the impact of porosification on a full LED structure and to demonstrate a fully porous LED. In this work, we have grown and analysed a porous LED fabricated by high temperature selective area sublimation. The structural analyses reveal a double porosity in the active region and in the GaN buffer. Cathodoluminescence mapping and electron beam induced current microscopy is used to probe the impact of porosification on the optical and electrical properties of the structure at nanoscale dimensions. A porous LED is fabricated using parylene pore filling and its electroluminescence is analysed.

RESULTS

LED growth, porosification and structural analyses. Two LED structures were grown in the same run in a 7×2 in. Aixtron AIX6 showerhead metal organic chemical vapor deposition reactor. Trimethylgallium (TMGa), triethylgallium (TEGa), trimethylindium (TMIn), trimethylaluminium (TMAl), bis(cyclopentadienyl)magnesium (Cp_2Mg), silane (SiH_4) and ammonia (NH_3) were used as the precursors for Ga, In, Al, Mg, Si, and N, respectively. The growth temperatures were measured by pyrometry using a reflectivity corrected system from Laytec. The epitaxial stack consists of (starting from the substrate) a 250 nm AlN buffer layer, 200 nm of undoped GaN, 400 nm of n-GaN, 20 nm of n-$Al_{0.05}Ga_{0.95}N$, 10 nm of n-GaN, a superlattice (SL) composed of 10 periods of 2.3 nm $In_{0.05}Ga_{0.95}N$ and 2.3 nm of GaN, 13 nm of an undoped GaN layer, a 4 periods multiple quantum well (MQW) consisting of 3.3 nm $In_{0.13}Ga_{0.87}N$ quantum wells and 13 nm quantum barriers, 100 nm of p-GaN and a last 15 nm p^{++} GaN contact layer. The p-doping activation is performed in situ immediately after the growth under a pure N_2 atmosphere at 750°C. The sample structure is illustrated in Figure 1a. The thicknesses were extracted from cross-section transmission electron microscopy images and the compositions of the different layers were measured by energy dispersive X-Ray spectroscopy (EDS).

The total epitaxial thickness is 1.1 µm which is much thinner than the 3.5–5.0µm typically requested for high efficiency blue LEDs on Si substrates.[10,12] Indeed, decreasing the total thickness of the structure can be an asset in order to decrease the total growth time. The purpose of the n-AlGaN below the SL is to act as a sublimation stop layer, however we will see in the following that locally the selective area sublimation process used to porosify the sample can go through this layer, probably due to an insufficiently high Al composition. The SL is expected to trap GaN surface defects in order to enhance the efficiency of the InGaN/GaN MQW as explained in Ref. 13. Compared to regular InGaN-based LED structures, no AlGaN electron blocking layer is inserted between the MQW and the p-GaN. The Al composition of this layer has to be typically in the 0.15–0.20 range and with such a composition the sublimation would be stopped at this layer.

In the following we present a comparison of one LED wafer that was kept as a reference and the second one which was processed in a Riber molecular beam epitaxy system for the porosification. The first step of the porosifi-

cation process is to form a Si_xN_y nanomask at the surface of the LED structure. The sample is annealed under 100 standard cubic centimeters per minute of ammonia at 800°C during 10 minutes in order to remove possible surface contaminants due to the sample transfer in the air. It was verified that after this annealing a clear 2×2 reflection high energy electron diffraction pattern (RHEED) was observed below 550°C, attesting that the GaN surface was well deoxidized. Then the sample is heated at 670°C under vacuum and exposed to the flux from a Si cell heated at 1250°C for 35 minutes. At this stage, a faint $\sqrt{3} \times \sqrt{3}R30°$ surface reconstruction was observed on the RHEED pattern and was related to the formation of Ga/Si-N bonds.[14] Note that it was not necessary to provide an additional nitrogen source to form this layer, the nitrogen already present at the surface or coming from the background residual ammonia pressure in the reactor (10^{-9} to 10^{-8} Torr) was sufficient. The temperature of the sample is finally increased to 870°C, still under vacuum, for 480 minutes in two consecutive runs. During this last step, the sublimation occurs in areas not covered by the Si_xN_y nanomask as explained in more details in our previous works.[9,15–17]

As explained in the Supplementary Materials, the pore density presents a variation over the 2 inch wafer between the center and the edge. After optical analyses of different places described in Supplementary Materials, regions with medium and low porosity were selected for further characterizations and the low porosity part was chosen for the device fabrication.

First, electron microscopy analyses of the structure were performed. The investigations were carried out by scanning electron microscopy (SEM) in the dual beam FEI Helios NanoLab and next in the JEOL ARM 200 atomic resolution scanning transmission electron microscope (STEM) for EDS and imaging. In the focused ion beam (FIB), we prepared the plane-view and cross section samples, using focused Ga beams with energies that are varied from 30 down to 1 kV for final polishing and minimizing the beam generated damage. The thinning process is closely monitored; during the process, primary structural and chemical information is systematically acquired using the electron beam in the scanning mode and finally in the scanning transmission mode when the lamella is thin enough for transparency to the 30 kV electron beam usable in the SEM mode of the FIB.

For the LED wafer which was subjected to porosification, the structure can be seen in the low magnification STEM image of Figure 1b, where the active area of InGaN/GaN QWs is indicated by horizontal black arrows. Inside the GaN template and surface layers, the contrast changes are due to thickness changes and therefore to the porosity. As can be seen, the porosity is much more extended in the GaN template, and in this cross-section projection the pores appear much larger. There is an abrupt transition at the level of the AlGaN layer which starts the active region as indicated by the arrows from Figure 1b to Figure 1a. This difference is better seen in plane-view SEM observations as shown in Figures 1c and Figure 1d. In the surface region (Figure 1c), the pores are rather small (darkest contract) and their morphology is highly complex, in contrast, the GaN template exhibits large pores with the geometry following the original distribution of dislocations as sub grain boundaries (Figure 1d). The higher magnification STEM image of Figure 1e helps to explain what happens during the porosification. Inside the 20 nm thick $Al_{0.05}Ga_{0.95}N$ layer, the large pores from the GaN template as well as most of the smaller ones from the GaN surface layer are stopped. As can be clearly seen, the pores from the surface straightforwardly cross the QWs, the SL and the first GaN 20 nm layers to stop inside the AlGaN layer. However, some of the pores cross the whole stacking down to the AlN buffer layer on top of the Si substrate (see white arrow in Figure 1b).

Figure 1f shows a high magnification image of the QW region. The QWs are continuous, however they display fluctuations of their thickness, EDS measurements give a maximum In composition of 15%, obtained in thicker areas of the QWs. In the observed areas, there is no obvious formation of extended defects, so the QWs are locally elastically strained. However, as can be seen at large scale in the SEM image of Figure 1c, numerous pores are formed in this area and their distribution is completely different from that in the underlying GaN template, so the strain has many channels of relaxation.

As pointed out in Figures 1b-e, the behavior during sublimation of the GaN template and of the upper active part is completely different. Large vertical pores of dendritic shape form inside the GaN template; they are fully stopped by the AlN buffer layer on top of the Si substrate, and are mainly stopped by the AlGaN interlayer under the active heterostructures. A close examination of Figures 1c-d shows that there are common features in the two figures which are recorded in the same sample area with FIB lamellas lifted-out respectively from the GaN template and from the surface region. In the surface region, we observe localized pores that have the form of round dots or small segments (the darkest contrast in Figure 1c). For the GaN template, as can be seen in Figure 1d, the pores are large and they exhibit large dendritic shapes, in contrast to the surface area, where the pores are small. Therefore, there is a large change in the porosification behaviour throughout the LED stack, which can be related with the dislocation pattern. TEM examinations of the reference sample (detailed in Supplementary Materials) show that the heterostructure strongly modifies the defect distribution: the screw and mixed type dislocations[18,19] appear to cross the heterostructures almost vertically. The other detects should close or be highly modified at these interfaces,[20–22] while edge type dislocations[23] are strongly bent inside the interface heterostructures (see Figure S3 in Supplementary material). This bending leads to a random homogeneous distribution of edge dislocations at the surface. One can suggest that during the sublimation process, the porosification starts from the surface and takes place along all the dislocation lines leading to a large number of small pores at the surface. At the AlGaN layer, the cross-sectional observations (Figure 1b) show that many small pores are stopped, they most certainly correspond to the porosification through the dislocation lines that were strongly bent (cf. Supplementary Materials). For the dislocations lines that cross the active heterostructure without deviation, the

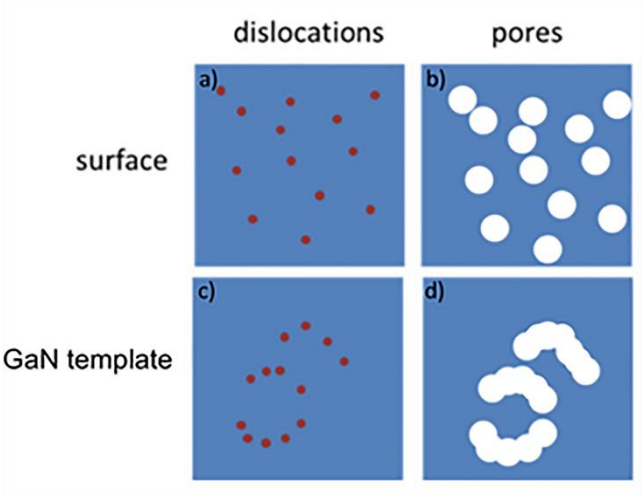

Figure 2. Schematic illustrating the formation of double porosity. (a) dislocation pattern at the surface. (b) formation of the small pores by sublimation from the surface. (c) dislocation pattern in the GaN template. (d) formation of big cavities in defective regions in the vicinity of the substrate.

AlGaN layer appears less effective and the porosification process continues towards the GaN template where it is amplified by the subgrain boundary configuration as seen in Figure 1d.

The mechanism leading to the observed difference in porosity may be explained with the following schematic shown in Figure 2. First small pores are initiated from the sample surface by sublimation of regions close to dislocations Figure 2a –b. These pores propagate downward by sublimation. Some of them are stopped by the AlGaN layer, however the composition of the AlGaN is not sufficient to block all the pores, so the pores associated with vertical dislocations can cross the AlGaN and propagate further into the GaN template. Finally, these pores reach highly defective regions in the vicinity of the substrate, where they are amplified by the subgrain boundary configuration and broaden into cavities Figure 2c – d.

Optical and electrical properties of the porous LED structure were characterized using CL mapping and EBIC microscopy and compared with the results for the reference structure, which was taken from the same wafer but has not undergone the sublimation process.

Cathodoluminescence mapping of the porous LED. CL maps were acquired using a CL-dedicated SEM (Attolight Allalin), with a beam energy from 3 to 5 keV and a beam current of approx. 4 nA. During experiments, the sample was maintained at a temperature of 10 K using a liquid Helium flow-cryostat. These conditions allowed to use short integration times, between 1 and 10 ms per spectral acquisition. The spectra were acquired with a Horiba iHR 320 monochromator using 600 groves per mm grating blazed for a wavelength of 300 nm. The signal was recorded by a charge coupled device (CCD) Andor Newton 920. The spectrometer setup has a spectral resolution of 0.13 nm.

First, top-view CL maps were recorded for the porous LED and for the non-porosified reference sample.

Figure 3a displays a low-temperature CL spectrum of the reference sample. The spectrum is integrated over a few square microns region shown in the SEM image of Figure 2b, which evidences the presence of pits at the surface. The spectrum shows two dominant emissions coming from the InGaN/GaN superlattice centered at 415 nm (2.99 eV) with a full width at half maximum (FWHM) of 98 meV and from the multi-quantum wells centered at 454 nm (2.74 eV) with a FWHM of 168 meV, respectively. Other contributions observed at higher energy are likely to be related with the DAP emission from GaN[24]. Figure 2c presents a CL map spectrally filtered for the InGaN/GaN QW emission peak. Strong intensity fluctuations are observed on submicrometer scale, which are partly correlated with the density of V-pit defects seen in the SEM image. These fluctuations are visualized in the histogram showing the distribution of pixel intensity of the map. The intensity fluctuations are also accompanied with a strong local shift of the QW peak in the 440-460 nm range (shown in panel d), which can be attributed to different effects like the In content variation, to the QW thickness fluctuation and to the inhomogeneous strain state in the vicinity of the defects. This is illustrated by a broad distribution of the peak energy for individual pixels shown on the histogram at the color bar.

The same analyses were performed for the porous LED. Figure 3e presents the integrated spectrum for the region shown in panel f. The superlattice emission is peaked at 401 nm (3.09 eV) with a FWHM of 78 meV and the QW peak is located at 446 nm (2.78 eV) with a FWHM of 134 meV. The superlattice peak and the QW peak are blueshifted with respect to the reference sample. This can be attributed to the strain relaxation leading to the reduction of the internal field and of the quantum confined Stark effect. Compared to the reference sample, a reduction of the peak broadening both for the SL and for the QW emission is observed in porous LED. This favourable effect of porosification can also be seen in the peak wavelength map in panel h showing local peak shifts. This can be associated with the sublimation of defective areas in the vicinity of pit defects, which are associated with the variation of the InGaN content and strain state. This is reflected by a narrower distribution of the peak energy for individual pixels compared to the reference sample as shown on the histogram at the color bar of panel (h).

Figure 3g presents the CL map of the porous LED spectrally filtered for the emission of the active QWs. Intensity fluctuations are observed with a characteristic spatial scale similar to that of the reference sample. However, the intensity fluctuations remain strong as seen from the intensity histogram on the color scale bar of panel (g). The comparison of the SEM image and the CL map does not show a correlation between the intensity of the QW emission and the pores. The CL inhomogeneities are observed at a different scale than the pores, they arise from the initial growth and are not produced by the porosification process.

Figure 4 presents the cross-sectional CL analyses of the reference sample and of the porous LED, which allow to localize the spatial origin of different spectral contributions.

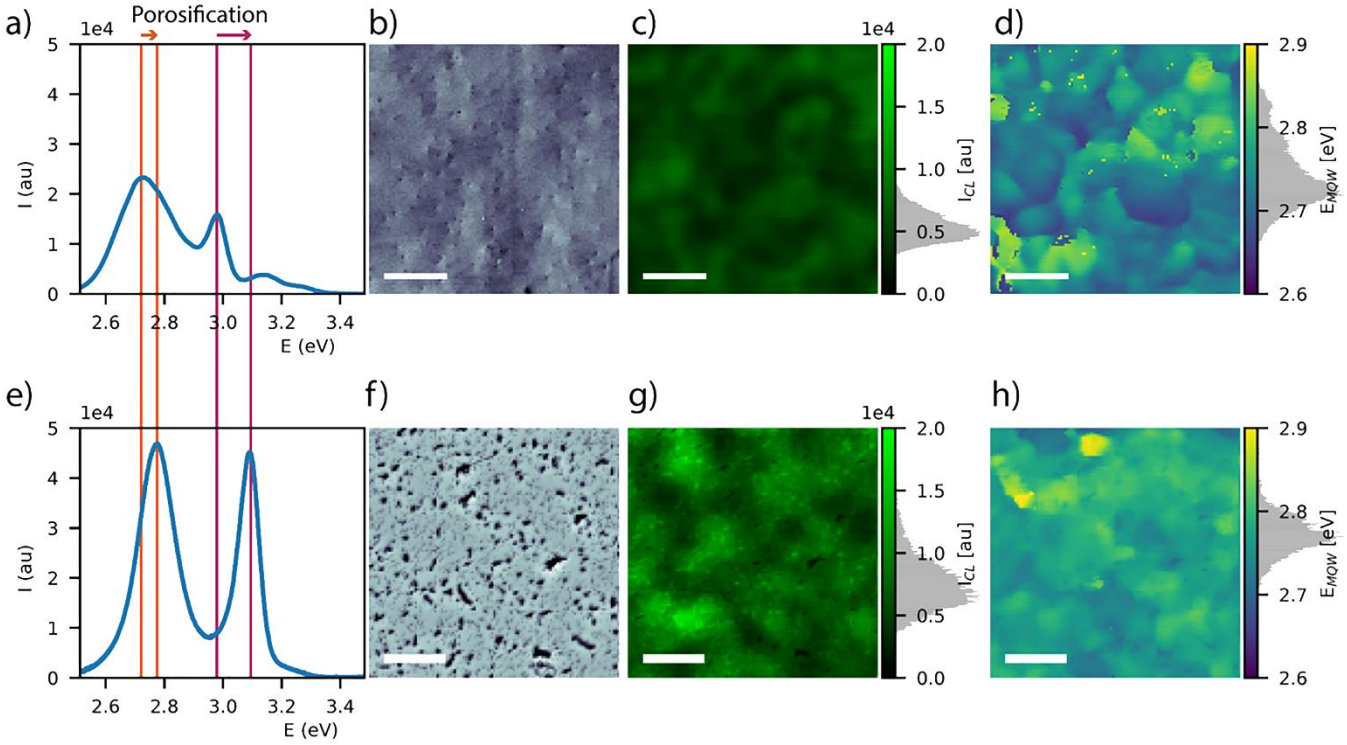

Figure 3. (a) and (e) integrated CL spectrum at 10 K; (b) and (f) SEM picture (c) and (g) CL map spectrally filtered for the QW emission peak. (d) and (h) Maps displaying the peak wavelength. The historiagrams on the color scale represent the distribution of pixel intensity in (c) and (f) and of the pixel energy in (d) and (h). Panels (a) – (c) refer to the reference sample, panels (d) – (f) refer to the porous LED. The scale bar is 500 nm.

Figure 4a and b show the cross-sectional SEM and the respective filtered map for the emissions of the super-lattice (between 400 and 430 nm, shown in blue) and of the active QWs (430 and 480 nm, shown in green) for the reference sample. Strong intensity fluctuations in the QW plane are observed, some of them may be related to the cleavage imperfections while others originate from non-radiative defects in the layers. The cross-sectional SEM of the porous LED shown in Figure 4c evidences the above described double porosity. The super-lattice and the QW emissions can be easily localized in the CL map, they are located close to each other just above the porosity change in agreement with the structural analyses discussed in Figure 1. Intensity fluctuations in the QW plane are also observed, however, with respect to the reference sample, the emission of the porous LED is more homogeneous.

To summarize, the top-view and cross-sectional CL analyses show that the high temperature sublimation process does not degrade the QW emission. On the contrary, a narrowing of the QW peak and a better spatial homogeneity is observed after porosification.

EBIC on the cross-section. Electron-beam induced current (EBIC) microscopy was applied to the porous LED and to the reference sample in order to probe the effect of porosification on the electrical properties of the p-n junction. The Hitachi SU8000 SEM microscope equipped with a Kleindiek micro probe-station was used for sample analyses (for details see setup description in Ref. 25). The EBIC measurements were performed at room temperature using an acceleration voltage of 25 kV. This high acceleration voltage was chosen to probe the sample in-depth and to be less sensitive to the surface morphological imperfections. For cross-sectional measurements, the samples were cleaved, contacted on their bare top p-GaN surface with a nano-probe, while the bottom contact is provided by the substrate connected to the ground. A reverse bias of -1 V was applied to the sample to overcome the Schottky barrier between the probe and the p-doped GaN on the sample

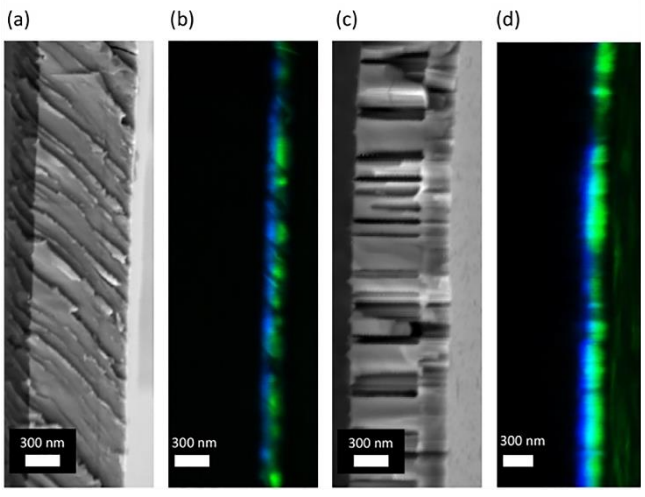

Figure 4. (a) Cross-sectional SEM image of the reference sample (surface is on the right) and (b) the corresponding spectrally filtered CL map at 10 K for the emission of the SL (blue) and of the QWs (green), respectively. (c) Cross-sectional SEM image of the porous LED (surface is on the right) and the corresponding (d) spectrally filtered CL map at 10 K for the emission of the SL (blue) and of the QWs (green), respectively.

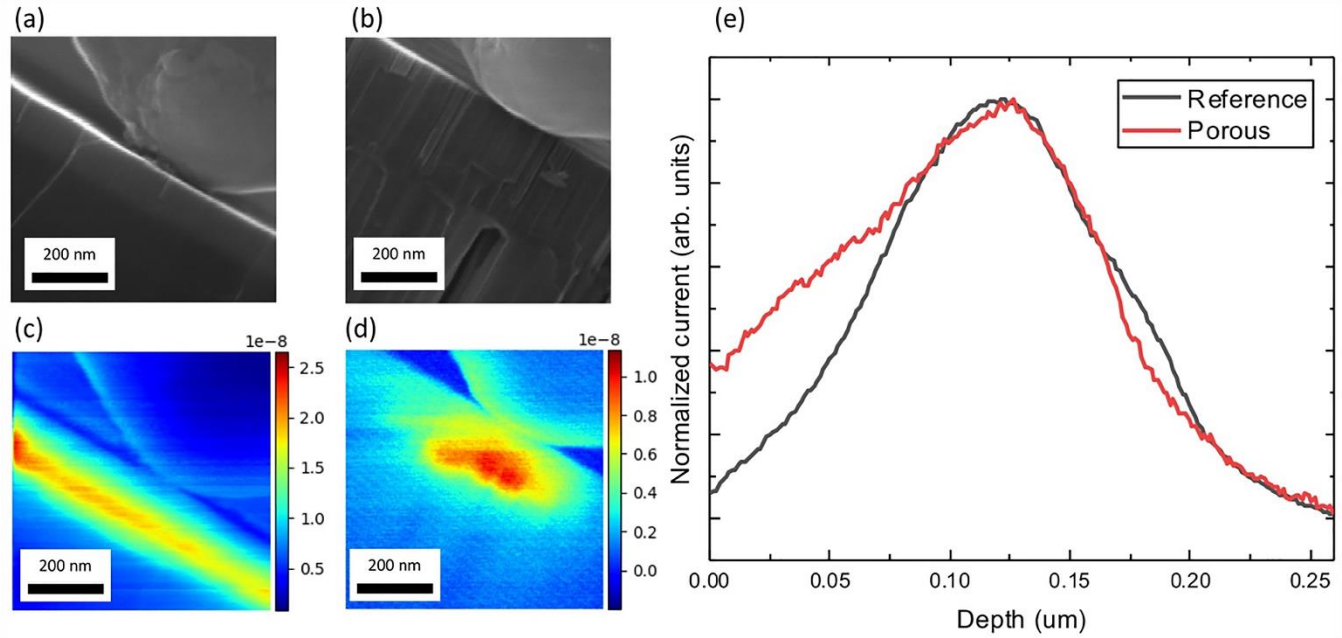

Figure 5. Cross section SEM (a) of the reference and (b) of the porous LED, corresponding EBIC maps under -1 V bias (c) of the reference and (d) of the porous LED (color scale shows the induced current in Amp). (e) EBIC profiles perpendicular to the layer plane of the reference and of the porous LED (sample surface corresponds to 0 μm).

surface and thus to improve the signal-to-noise ratio. To measure the induced current, a low noise current preamplifier SR570 coupled with a Gatan Digiscan system was used. The EBIC maps were constructed point by point by scanning the sample surface. Figures 5a and c show the SEM image and the induced current map for the reference sample. The maximum of the signal corresponds to the nominal position of the active QWs located in the depleted region of the p-n junction and the signal quickly decreases in the p-GaN top layer and the n-doped bottom layer (cf. the EBIC profiles of Figure 5e). In the junction plane the EBIC signal is rather homogeneous evidencing efficient in-plane current collection. For the porous LED analyses shown in Figure 5b and d, the induced current can only be collected in the vicinity of the probe – the in-plane signal extension is smaller than 0.5 μm. This is indeed expected since the porosification reduces the in-plane conductivity due to the creation of holes in the p-GaN layer. At the same time, the in-depth EBIC profile of the porous LED is similar to the one observed for the reference sample. The position of the signal maximum is the same, which shows that the doping profile of the p-n junction is not much affected by the high temperature sublimation process. This is important since one could have expected some interdiffusion or other electrical degradation due to the long high temperature annealing. The decrease of the EBIC signal in the n-doped bottom layer has the same shape as for the reference sample. However, in the p-GaN part the profile shape is different, the decrease of the signal is non-exponential, which may be related to the modification of the electrical properties on the p-GaN layer. Indeed, an exponential profile is expected in situations when a unidimensional diffusion model is applicable, which is not the case of a porous material where the transport of minority carriers can be three-dimensional.

Overall, the comparative EBIC analyses demonstrate that the high temperature sublimation process preserves the electrical activity of the p-n junction, which is favorable for device fabrication.

LED fabrication and testing. To process the porous LED the low porosity (8%) region was selected. A special care should be taken to electrically insulate the pores to avoid short-circuiting. To fill the pores, a 2 μm thick layer of parylene-C was deposited on the top surface. Then, the excess of the parylene was etched by an oxygen plasma to uncover the p-GaN top surface. Due to the inhomogeneities of the pores density through the wafer, the resulting parylene coverage was not homogeneous, therefore the central part of the sample with the optimal pore filling was selected for characterization. The top transparent contact to the LED was defined using optical lithography, ITO sputtering and lift-off. Finally, a metal frame was deposited for device bonding purposes. The bottom contact was take on the Si substrate. Figure 6a shows the schematic of the porous LED. First, the fabrication process was validated by electrical measurements and EBIC microscopy. Figures 6b and c show the SEM image and the corresponding EBIC map of a region on the top surface of the LED covered with ITO. The induced current shows dips in the pores since the p-n junction is removed by sublimation. However, these dips affect only the pores and not the neighboring regions, where the induced current shows only slow variations. This shows the absence of local shunts through the pores and demonstrates that the pores do not affect the current generated in the neighbouring region of the p-n junction. Based on this observation we can assume that the eventual non-radiative recombination on the pore sidewalls is relatively low since it does not change the collection of the minority carriers in the pore vicinity. This is further confirmed by the room-temperature CL mapping of the analyzed LED, shown in Figure2S of Supplementary Materials.

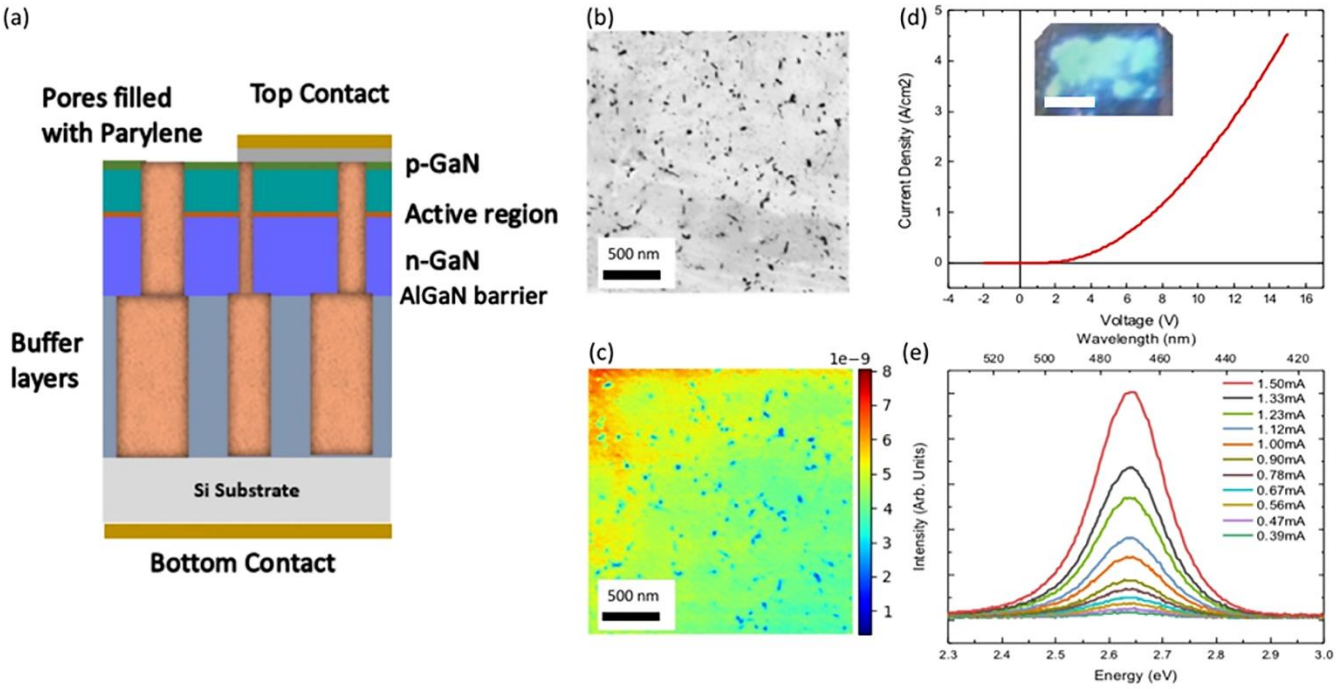

Figure 6. (a) Schema of the porous LED after fabrication. (b) top-view SEM image and (c) the corresponding EBIC map of the porous LED. (d) I-V curve of the porous LED with a photo of the device under operation, the scale bar is 150 µm, and (e) electroluminescence spectra for different injection currents.

The fluctuations of the CL intensity are not correlated with the pores, in particular no drop of the luminescence in the pore vicinity is observed.

The LED presents a rectifying diodic current-voltage (I-V) characteristic (cf. Figure 6d), which again confirms that the parylene pore protection is efficient and the device is not short-circuited. The reverse leakage of the LED is relatively low (1 mA/cm2 at -2 V).

The electroluminescence (EL) spectra of the LED were recorded for increasing injection current as shown in Fig. 6 (e). The EL is peaked at 2.635 eV with a FWHM of 170 meV. The peak position shows only a negligible blueshift for increasing injection (going from 2.630 eV for 0.4 mA to 2.637 for 1.5 mA). This low blueshift compared to standard non-porous LEDs[26] is consistent with the reduction of the internal electric field in the QWs thanks to porosification. The inset of Figure 5c shows an optical microscopy image of the LED under operation, showing intensity fluctuations. These fluctuations of the electroluminescence are tentatively attributed to electrical inhomogeneities of the top contact, which may be caused by parylene residues on the surface due to insufficient etching. Further optimization of the parylene planarization step is expected to solve the issue.

Conclusion. A fully porous LED obtained by high temperature sublimation was fabricated and analysed. A change of porosity between the active region and the GaN buffer was observed. This phenomenon is explained by the modification of the dislocation pattern in the heterostructure, which is evidenced by weak beam transmission electron microscopy on the non-porosified reference sample. The impact of high temperature sublimation on the optical and electrical properties of the LED structure is assessed using cathodoluminescence and electron beam induced current microscopy. It is observed that neither QW emission nor the p-n junction EBIC spatial profile were degraded after porosification with respect to the non-annealed reference sample. A LED is demonstrated using parylene insulation of the pores and its electroluminescence is analyzed. To the best of our knowledge, it is the first report of an InGaN-based LED with a fully porous active region.

ASSOCIATED CONTENT

Supporting Information. Cathodoluminescence characterization of region with different porosities as well as TEM analyses of dislocations in the reference LED (PDF). This material is available free of charge via the Internet at http://pubs.acs.org.

AUTHOR INFORMATION

Corresponding Author

Maria Tchernycheva – Centre de Nanosciences et de Nanotechnologies (C2N), Univ. Paris-Saclay, UMR 9001 CNRS, Palaiseau 91120, France; https://orcid.org/0000-0003-4144-0793; Email: maria.tchernycheva@universite-paris-saclay.fr

Author Contributions

The manuscript was written through contributions of all authors. All authors have given approval to the final version of the manuscript.

Notes

The authors declare no competing financial interest.

Data Availability. The data that support the findings of this study are available from the corresponding author upon request.

ACKNOWLEDGMENT

This research was supported by ANR Napoli ANR-18-CE24-0022 and Labex GANEX (grant no. ANR-11-LABX-0014). NT and AFM thank SNSF for funding through Bridge project nr 40B2-0_176680. For the TEM sample preparation, this work acknowledges the use of the SEM/FIB FEI Nanolab 660, which is a facility acquired in the scope the EQUIPEX GENESIS, N°ANR-11-EQPX-0020 under the "Investissements d'avenir" national Programme.

REFERENCES

(1) Monaico, E.; Tiginyanu, I.; Ursaki, V. Porous semiconductor compounds. *Semicond. Sci. Technol.* **2020**, *35* (10), 103001. DOI: 10.1088/1361-6641/ab9477

(2) Kochergin, V. and Föll H., *Porous Semiconductors: Optical Properties and Applications.* Springer-Verlag: London, 2009, 209. DOI: 10.1007/978-1-84882-578-9

(3) Hartono, H.; Soh, C. B.; Chow, S. Y.; Chua, S. J.; Fitzgerald, E. A. Reduction of threading dislocation density in GaN grown on strain relaxed nanoporous GaN template. *Appl. Phys. Lett.* **2007,** *90* (17), 171917. DOI: 10.1063/1.2732826

(4) Soh, C. B.; Tay, C. B.; Tan, R. J. N.; Vajpeyi, A. P.; Seetoh, I. P.; Ansah-Antwi, K. K.; Chua, S. J. Nanopore morphology in porous GaN template and its effect on the LEDs emission *J. Phys. D: Appl. Phys.* **2013**, *46* (36), 365102. DOI: 10.1088/0022-3727/46/36/365102

(5) Lee, K. J.; Kim, S.-J.; Kim, J.-J.; Hwang, K.; Kim, S.-T.; Park, S.-J. Enhanced performance of InGaN/GaN multiple-quantum-well light-emitting diodes grown on nanoporous GaN layers *Opt. Express* **2014**, *22* (S4), A1164. DOI: 10.1364/OE.22.0A1164

(6) Griffin, P. H.; Oliver, R. A. Porous nitride semiconductors reviewed *J. Phys. D: Appl. Phys.* **2020**, *53* (38), 383002. DOI: 10.1088/1361-6463/ab9570

(7) Kao, C.-C.; Huang, H. W.; Tsai, J. Y.; Yu, C. C.; Lin, C. F.; Kuo, H. C.; Wang, S. C. Study of dry etching for GaN and InGaN-based laser structure using inductively coupled plasma reactive ion etching *Mater. Sci. Eng.: B* **2004**, *107* (3), 283–288. DOI: 10.1016/j.mseb.2003.11.023

(8) Pasayat, S. S. et al. Color-tunable <10 μm square InGaN micro-LEDs on compliant GaN-on-porous-GaN pseudo-substrates *Appl. Phys. Lett.* **2020** *117* (6), 061105. DOI: 10.1063/5.0011203.

(9) Damilano, B.; Vézian, S.; Massies, J. Photoluminescence properties of porous GaN and (Ga,In)N/GaN single quantum well made by selective area sublimation *Opt. Express* **2017,** 25 (26), 33243. DOI: 10.1364/OE.25.033243

(10) Zhang, L.; Tan, W.-S.; Westwater, S.; Pujol, A.; Pinos, A.; Mezouari, S.; Stribley, K.; Whiteman, J.; Shannon, J.; Strickland, K. High Brightness GaN-on-Si Based Blue LEDs Grown on 150 mm Si Substrates Using Thin Buffer Layer Technology *IEEE J. Electron Devices Soc*. **2015**, *3* (6), 457–462. DOI: 10.1109/JEDS.2015.2463738

(11) Bilousov, O. V. et al. Fully Porous GaN p–n Junction Diodes Fabricated by Chemical Vapor Deposition *ACS Appl. Mater. Interfaces* **2014,** *6* (20), 17954–17964. DOI: 10.1021/am504786b

(12) Nunoue, S. et al. LED manufacturing issues concerning gallium nitride-on-silicon (GaN-on-Si) technology and wafer scale up challenges in *2013 IEEE International Electron Devices Meeting*, Washington, DC, USA, 9-11 Dec. 2013 p. 13.2.1-13.2.4. DOI: 10.1109/IEDM.2013.6724622

(13) Hallera, C.; Carlin, J.-F.; Jacopin, G.; Liu, W.; Martin, D.; Butté, R.; Grandjean, N. GaN surface as the source of non-radiative defects in InGaN/GaN quantum wells *Appl. Phys. Lett.* **2018,** *113* (11), 111106. DOI: 10.1063/1.5048010

(14) Markurt, T. et al. Blocking Growth by an Electrically Active Subsurface Layer: The Effect of Si as an Antisurfactant in the Growth of GaN *Phys. Rev. Lett.* **2013**, *110* (3), 036103. DOI: 10.1103/PhysRevLett.110.036103

(15) Damilano, B.; Vézian, S.; Brault, J.; Alloing, B.; Massies, J. Selective Area Sublimation: A Simple Top-down Route for GaN-Based Nanowire Fabrication *Nano Lett.* **2016,** *16* (3) 1863–1868. DOI: 10.1021/acs.nanolett.5b04949

(16) Damilano, B.; Vézian, S.; Massies, J. Mesoporous GaN Made by Selective Area Sublimation for Efficient Light Emission on Si Substrate *Phys. Status Solidi B* **2018,** *255* (5), 1700392. DOI: 10.1002/pssb.201700392

(17) Damilano, B.; Vézian, S.; Portail, M.; Alloing, B.; Brault, J.; Courville, A.; Brändli, V.; Leroux, M.; Massies, J. Optical properties of $In_xGa_{1-x}N$/GaN quantum-disks obtained by selective area sublimation *J. Cryst. Growth* **2017**, *477*, 262–266. DOI: 10.1016/j.jcrysgro.2017.01.010

(18) Ning, X. J.; Chien, F. R.; Pirouz, P.; Yang, J. W.; Khan, M. A. Growth defects in GaN films on sapphire: The probable origin of threading dislocations *J. Mater. Res.* **1996**, *11* (3), 580–592. DOI:10.1557/jmr.1996.0071

(19) Potin, V.; Vermaut, P.; Ruterana, P.; Nouet, G. Extended defects in wurtzite nitride semiconductors. *J. Electron. Mater.* **1998**, *27* (4), 266–275. DOI: 10.1007/s11664-998-0398-3

(20) Ruterana, P. et al. Formation mechanism and relative stability of the {112$\bar{0}$} stacking fault atomic configurations in wurtzite (Al, Ga, In) nitrides. *Phys. Rev. B* **1999**, *59* (24), 15917.

(21) Lacroix, B.; Chauvat, M. P.; Ruterana, P.; Nataf, G.; De Mierry, P. Efficient blocking of planar defects by prismatic stacking faults in semipolar (1122)-GaN layers on m-sapphire by epitaxial lateral overgrowth *Appl. Phys. Lett.* **2011**, *98* (12), 121916. DOI: 10.1063/1.3571455

(22) Potin, V., Nouet, G., Ruterana, P. The {1010} inversion domains in GaN/sapphire layers: An electron microscopy analysis of the atomic structure of the boundaries. *Philos. Mag. A* **1999**, *79* (12), 2899–2919. doi:10.1080/01418619908212032

(23) Potin, V.; Ruterana, P.; Nouet, G.; Pond, R. C.; Morkoç, H. Mosaic growth of GaN on (0001) sapphire: A high-resolution electron microscopy and crystallographic study of threading dislocations from low-angle to high-angle grain boundaries. *Phys. Rev. B* **2000**, *61* (8), 5587–5599. DOI: 10.1103/physrevb.61.5587

(24) Díaz-Guerra, C.; Piqueras, J.; Castaldini, A.; Cavallini, A.; Polenta, L. Defect assessment of Mg-doped GaN by beam injection techniques *J. Appl. Phys.* **2003**, *94* (12), 7470–7475. DOI: 10.1063/1.1628832

(25) Lavenus, P.; Messanvi, A.; Rigutti, L.; De Luna Bugallo, A.; Zhang, H.; Bayle, F.; Julien, F. H.; Eymery, J.; Durand, C.; Tchernycheva, M. Experimental and theoretical analysis of transport properties of core–shell wire light emitting diodes probed by electron beam induced current microscopy *Nanotechnology* **2014**, *25* (25), 255201. DOI: 10.1088/0957-4484/25/25/255201

(26) Chichibu, S. F. et al. Optical properties of InGaN quantum wells in *Materials Science and Engineering B: Solid-State Materials for Advanced Technology* **1999**, *59* (1–3), 298–306. DOI: 10.1016/S0921-5107(98)00359-6

SYNOPSIS TOC.